Nanoscale

Accepted Manuscript

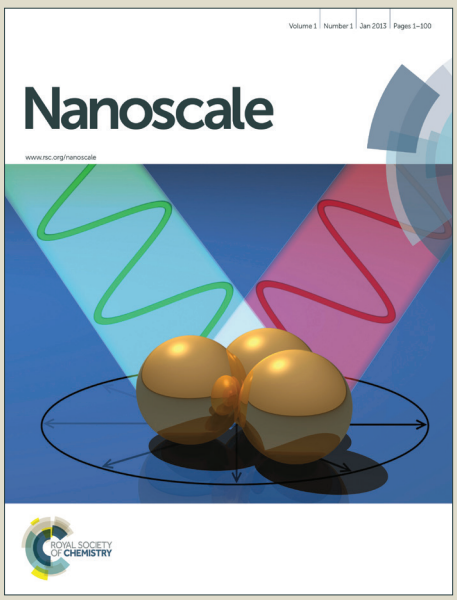

ROYAL SOCIETY OF CHEMISTRY

www.rsc.org/nanoscale

Journal Name

ARTICLE

Enhanced oxidation-resistance Cu-Ni core-shell nanowires: Controllable one-pot synthesis and solution processing to transparent flexible heaters

Received 00th January 20xx,
Accepted 00th January 20xx

DOI: 10.1039/x0xx00000x

www.rsc.org/

Jianyu Chen[§, a], Jun Chen[§, a], Yi Li[§, a], Weixin Zhou[a], Xiaomiao Feng[a], Qingli Huang[b], Jian-Guo Zheng[*, c], Ruiqing Liu[a], Yanwen Ma[*, a], Wei Huang[a]

Abstract: Coating nickel onto copper nanowires (Cu NWs) by one-pot synthesis is an efficient approach to improving the oxidation resistance of the nanowires. Because Ni is much less conductive than Cu, it is of great importance to understand the relationship between the thickness of Ni coating layer and the properties of NWs. Here we demonstrate one-pot synthesis of Cu-Ni core-shell NWs with tunable Ni thickness by simply varying Cu and Ni mole ratio in precursor. We have observed that increasing Ni thickness decreases the aspect ratio, surface smoothness and network conductivity of the resulting NWs. However, Cu-Ni NWs with thicker Ni layer display higher oxidation temperature. The optimal Cu-Ni NWs, which were prepared using Cu^{2+}/Ni^{2+} molar ratio of 1/1, have the Ni-layer thickness of about 10 nm and the onset oxidation temperature of 270 °C. The derived transparent conductive films present transmittance of 76 % and sheet resistance of 300 Ω /sq. The flexible heater constructed from such high quality Cu-Ni NW films demonstrates effective performance in heating and defrosting.

Introduction

During past few years, various efforts have been made to explore new transparent conductive materials for replacing indium tin oxide (ITO), a brittle, scarce and expensive electrode material.[1-3] Of various alternatives, metal nanowires (NWs), typically Ag NWs can achieve performance comparable to ITO.[4-5] In addition, Ag NWs are not only more flexible and stretchable than ITO, but also can be processed in solution to meet the needs of roll-to-roll manufacturing.[6-8] Up to date, Ag NW-based transparent conductive films (TCFs) can reach a sheet resistance below 10 Ohm/sq at a transmittance higher than 95%,[9] making them applicable in organic light-emitting diodes,[10-12] organic photovoltaics,[13-15] touch-screens[16-17] and defrosting windows.[18-19] However, the price of silver is even higher than ITO, which presents a major bottleneck for their industrial applications. Since copper is only 6% less conductive but much cheaper than silver,[20] Cu NWs have been extensively investigated to replace Ag NWs in recent years.[21-30] With continues refinement and improvement, Wiley and his colleagues have synthesized high aspect ratio Cu NWs in aqueous solution and prepared TCFs with a transparency of 90% at 45 Ω sq^{-1}.[23] High-quality Cu NWs can also be synthesized in organic oleylamine solvent, but the solidification of oleylamine at ambient temperature makes the final purification difficult.[24] Compared with Ag NWs, Cu NWs are more sensitive to the oxidation of oxygen and moisture,[24, 26-32] which is the main obstacle that impedes their application in some devices, such as transparent heaters. Hence, it is highly required to significantly improve the oxidation resistance of Cu NWs. Coating oxidation-resistance metal layers, e.g., Au layer, is a general strategy to improve the stability of Cu nanocrystals.[33] One route developed by Wiley et al. is electroless plating of nickel, cobalt and other metals on the synthesized Cu NWs to form core-shell (cable) structure.[26-30] The Cu-Ni NWs exhibited remarkable stability and even 100 times higher resistance to oxidation than Ag NWs.[26] However, during electroless-plating process, the deposition of nickel is performed without the confinement of molecular templates or capping agents, leading to rough surfaces of the synthesized nanowires.[27] As a result, the electrical conductivity of such NWs is reduced due to the dramatic increase of surface scattering of electrons. The rough surfaces also induce the scattering of light, hereby deteriorating the transparency of the corresponding TCFs. Additionally, the unavoidable oxidation of the surfaces of the pre-formed Cu NWs results in

[a] Key Laboratory for Organic Electronics and Information Displays & Institute of Advanced Materials (IAM), Jiangsu National Synergistic Innovation Center for Advanced Materials (SICAM), Nanjing University of Posts and Telecommunications, 9 Wenyuan Road, Nanjing 210023, China. *email: iamywma@njupt.edu.cn.
[b] Testing center, Yangzhou University, Yangzhou city, Jiangsu 225009, China
[c] Irvine Materials Research Institute (IMRI), University of California, Irvine, CA 92697, USA *email:jzheng@uci.edu,
§ These authors contributed equally to this work.

†Electronic Supplementary Information (ESI) available: Detailed experimental conditions, SEM images and EDS element maps of other Cu-Ni NWs, Schematic of neat Cu and Cu-Ni NW growth process, TG and DTG curves of other Cu-Ni NWs, Flexibility tests, Photograph and SEM images of other Cu-Ni TCFs, Infrared thermal images of flexible heaters. See DOI: 10.1039/x0xx00000x

copper-oxidation interface layers of the target core-shell NWs and reduces their conductivity, which makes it absolutely essential to deposit protection layers on Cu NWs at the same time as the growth of the NWs. Fortunately, Zeng et al.[31] have already developed one-pot process to synthesize high-quality Cu-Ni NWs with smooth surface in 2010. Since nickel is much less conductive than copper, the Ni shell needs to be as thin as possible, meanwhile its oxidation-resistance capability still remains. Hence it is of great importance to optimize Ni-layer thickness if Cu-Ni NWs are used to prepare TCFs. In this work, we demonstrate one-pot synthesis of Cu-Ni core-shell NWs with tunable Ni-shell thickness. The Cu-Ni NWs with 10 nm thick Ni shell exhibit the optimal conductivity and oxidation resistance. The oxidation onset temperature is increased from 180 °C for neat Cu NWs to 270 °C for Cu-Ni NWs. Such high oxidation resistance owned by Cu-Ni NWs allows the solution processed TCFs to act as flexible heaters for defrosting windows.

Experimental

Preparation of Cu-Ni NWs

Copper nitride and nickel acetate with preset mole ratio (Table S1†in Supporting Information) were dissolved into 800 mL of high concentrated NaOH solution (7-12 mol L^{-1}) containing 3-12 mL ethylenediamine (EDA) and 1 mL hydrazine (35 wt%). Here EDA acts as capping agent and hydrazine is reductant. The mixed solution was heated to 60-80 °C and maintained for 60-120 min without stirring. All the reagents were purchased from Aladdin Chemistry and used without further purification. The as-prepared solid sample was separated by filtration and stored in acetone/ethanol solution.

Preparation of Cu-Ni NW TCFs

Cu-Ni NW ink was deposited onto poly(ethylene terephthalate) (PET) substrate to form a uniform thin film by spray coating. The density of nanowires on the surface was adjusted by varying the Cu-Ni NW concentration in the ink. The film was allowed to dry in air for 5–10 min and then mechanically pressed between two mirror surfaces of plastic mold steels at 8 MPa for 1 min.

Preparation of Cu-Ni NW heaters

A Cu-Ni NW film heater was prepared by attaching two strips of copper conductive strips on two opposite edges of a TCF (200 mm × 50 mm). The DC voltage was supplied by a power supply (Keithley 2400). The temperature of the film was measured using a thermal imager (FLIR) and the thermocouple was mounted on the top surface of the film. For the defrost test, the Cu-Ni NW film heater with a surface resistivity of 300 Ω sq^{-1} was placed for 30 min in a refrigerator set to −10 ℃ to induce frost on the film, then an input voltage of 12 V was applied to the two copper strips of the film heater.

Temperature profiles on the surface of the film were detected by a thermal imager (FLIR) at a given input voltage. The temperature measurements were performed with room temperature at 25 ℃, where the room temperature was controlled (±1℃) during measurements.

Instruments and characterization

Cu-Ni NWs were characterized by scanning electron microscopy (SEM, Hitachi S-4800), X-ray diffraction (XRD, Bruker D8 AdvanceA25 with Cu Kα radiation of 1.5418 Å), transmission electron microscopy (TEM, Hitachi 7700 operated at 120 kV), high-resolution TEM (HRTEM was done on a FEI Tecnai G2 F30 S-TWIN field-emission transmission electron microscope operated at 300 kV.) and energy-dispersive X-ray spectroscopy (EDS attached to FEI Talos TEM). Thermogravimetry analysis (Netzsch STA-449F3) was performed at a heating rate of 10 ºC min^{-1} in air. The transparencies of TCFs were measured by UV-Vis spectrophotometer (Shimadzu, UV-3600) and the sheet resistances were evaluated by four-point probe measurement (Keithley 2400 semiconductor parameter) at room temperature.

Results and discussion

The growth of neat Cu nanowires could be achieved in strong alkaline aqueous solution by reducing Cu^{2+} ions with hydrazine under the direction of ethylenediamine capping agent. EDA capping agent is easy to form complex ions with both Cu^{2+} and Ni^{2+} in strong alkaline solution in accordance with the coordination chemistry theory. $[Cu(EDA)2]^{2+}$ and $[Ni(EDA)3]^{2+}$ are expected to be present in solution precursors. (The standard reduction potential of $\mathbf{E^{\ominus}(Cu^{2+}/Cu)}$ =[+0.337 V] is much higher than $\mathbf{E^{\ominus}(Ni^{2+}/Ni)}$ =[-0.257 V] indicating that Cu^{2+} is easier to be reduced in competitive redox reactions).[34-35] Under similar experimental condition,[32] Cu-Ni core-shell NWs were feasibly synthesized from the co-reduction of Cu^{2+} and Ni^{2+} cations. The Ni content could be tuned by varying Cu^{2+}:Ni^{2+} molar ratios in precursors from 3:1 to 1:3 (Table S1). The NW composition was measured by sensitive EDS and the data are given in Table S2. The Cu-Ni NWs are named by their Cu/Ni molar ratios hereinafter. The products dispersed in ethanol solution clearly shows that their colors change from brownish red to dark gray with increasing Ni content (Fig. 1a). All the products maintain a wire-shaped morphology, but the nanowires prepared from Cu^{2+}/Ni^{2+} molar ratio of 1:1 or larger have much higher aspect ratio and smoother surface (Fig. 1b and Fig. S1† in Supporting Information). The Cu-Ni(1:1) nanowires have length of 20-40 μm and diameter of 70-100 nm (Fig. 1b and c). The crystal structures of these nanowires are well revealed in their XRD patterns (Fig. 1d). In Fig. 1d, each Cu-Ni related pattern presents two sets of diffraction peaks corresponding to metallic cubic Cu and Ni phases separately, indicating the bi-metallic phase structure of these nanowires.[36] It is clearly observed that the ratio of Cu/Ni peak intensity increases with increasing Cu^{2+}/Ni^{2+} molar ratio in the initial precursor solution, suggesting that the composition of Cu-Ni could be tuned as expected.

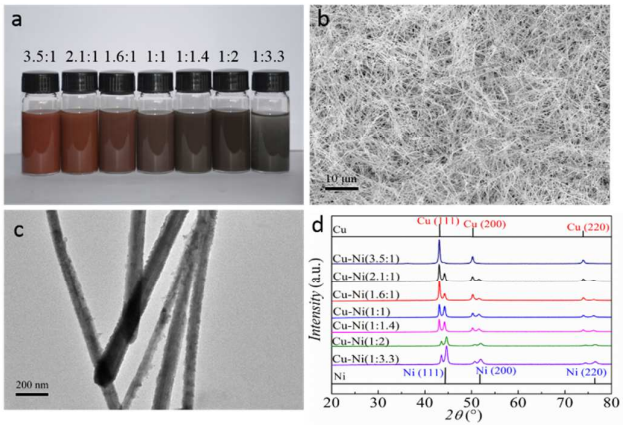

Fig1. a) Photograph of Cu-Ni nanowires with different Cu/Ni ratios (3.5:1，2.1:1，1.6:1，1:1，1:1.4，1:2，1:3.3), b) SEM image of Cu-Ni(1:1) NWs, c) TEM image of Cu-Ni(1:1) NWs, d) XRD patterns of all Cu-Ni NWs.

The microstructure of Cu-Ni NWs was studied by TEM, selected area electron diffraction (SAED), HRTEM and EDS related element mapping. Fig. 2a shows the bright field TEM image of one typical Cu-Ni(1:1) NW with the diameter of about 90nm and the inset is its corresponding SAED pattern. The SAED pattern displays two sets of diffraction spots, where some are indexed. The two sets of diffraction spots belong to the cubic zone axis [0$\bar{1}$1]. The lattice spacings measured from the spots indicate that the two sets of the spots are associated with metallic Cu and Ni respectively[37] and the spot arrangement shows that the corresponding lattice planes of Cu and Ni are parallel to each other. Because the lattice parameters of Cu are very closed to those of Ni (the difference <0.01nm), their low index spots are almost overlapped and only high index spots are separated. For an example, the separation of two 400 spots is distinguishable in the pattern. It is worthy to mention that the Cu 400 spot (closer to the direct beam or pattern center) is much stronger than the Ni 400 spot, indicating that the Cu content is much higher than Ni, which will be further confirmed by elemental maps. The SAED pattern also indicates that the growth direction of the nanowire is [011]. This is supported by HRTEM results. Fig. 2b (middle) displays the HRTEM image of the NW, which is from the area close to the wire edge as marked by the red rectangle lines in Fig. 1a. Enlarged HRTEM images are included to reveal more details of the core (Fig. 2b top right) and shell (Fig. 2b top left) structures. The two-dimensional lattice fringes of the Cu core and its Fast Fouries Transformation (FFT) pattern (Fig. 2b bottom right) indicate that the Cu core grows dominantly along the [011] direction while the electron beam (observation direction) is along the [0$\bar{1}$1] axis of Cu, which is perpendicular to the wire growth direction. It is a little complex in the shell area. As revealed in its FFT pattern (Fig. 2b bottom left), there are two sets of spots, one is related to Ni (a=0.352 nm) and another to NiO (a=0.417 nm). The corresponding lattice planes of Ni and NiO are parallel to each other, but the spacings are different. The large difference in lattice parameter enables us to distinguish Ni and NiO easily from in the enlarged HRTEM image (Fig. 2b top left), where the NiO (111) and Ni (111) planes have the interplanar spacings of 0.24nm and 0.20nm respectively. It is observed that NiO is on Ni surface and the thickness of the oxide layer varies from 2 to 6 nm (Fig. 2b middle). Some Moire fringes may be seen in the HRTEM image due to the overlapping of NiO and Ni. Because Cu (a=0.361 nm) and Ni (a=0.352nm) with the same face center cubic (fcc) structures have a small difference in their lattice parameters and are parallel to each other with their lattice planes, it is difficult to distinguish Cu and Ni in the HRTEM images. So EDS was used to reveal different elements. Fig. 2c shows a bright-field TEM image together with the element maps of Cu, Ni and O in the NW. It can be clearly seen that the Cu-Ni(1:1) NW has the core-shell structure and Ni layer covered with NiO is about 10 nm which is much smaller than the core dimension. This can be used to explain the intensity difference of 400 spots in SEAD pattern (Fig. 2a inset). By using the element-mapping technique, the core-shell structures of other Cu-Ni NWs are identified (Fig. S2†) as well. Moreover, these results reveal that the thickness of Ni layer could be successfully tuned from 0 to 15 nm by varying the content of Ni^{2+} precursor. In addition, these results also provide valuable information to deduce the possible growth process for Cu-Ni core-shell NWs (Fig. S3†).

Journal Name

ARTICLE

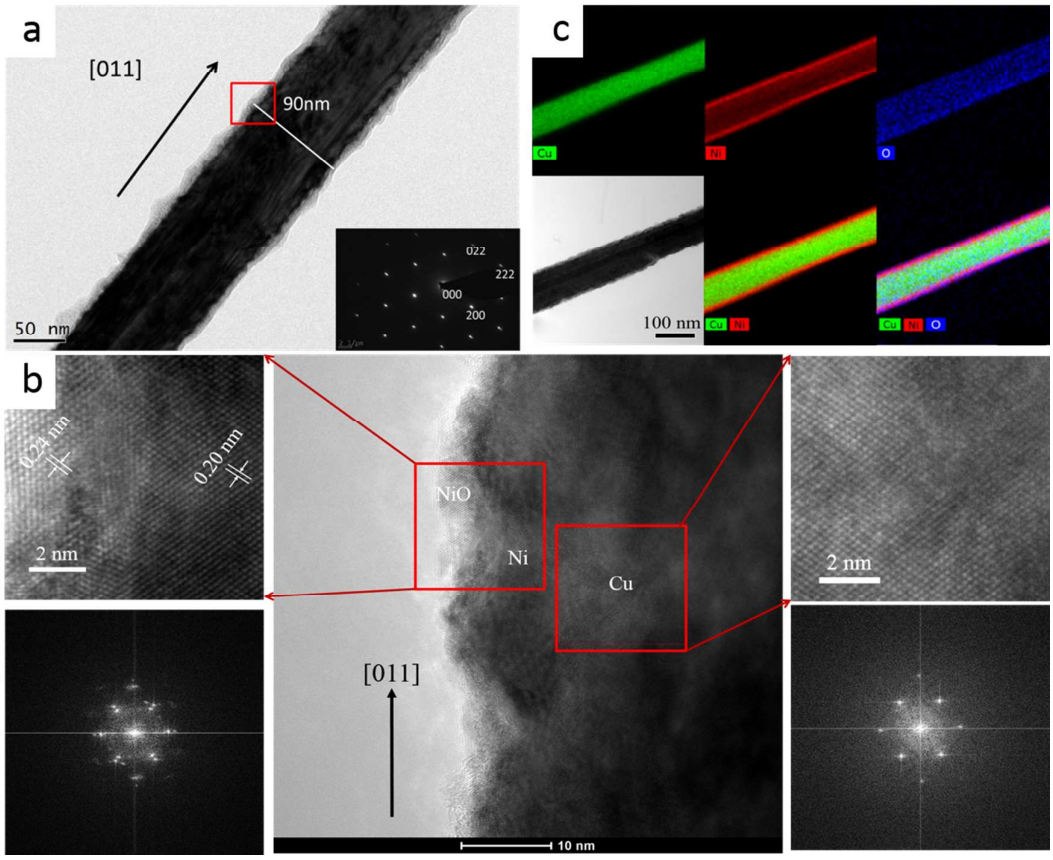

Fig2. (a) TEM image and SAED pattern of Cu-Ni NW with Cu/Ni molar ratio of 1:1; (b) HRTEM image of rectangle part in (a), local enlargements and FFT patterns of Cu and NiO/Ni zones; (c) TEM image and element maps.

The role of exterior Ni layer is to protect Cu NWs from oxidation when the wires are exposed in air. Fig. 3a shows thermogravimetry curves of neat Cu NWs and Cu-Ni(1:1) NWs that are examined in air from room temperature to 700 °C with a rate of 10 °C/min. The neat Cu NWs suffer a quick oxidation process starting at 180 ℃ and show a weight gain of 19 %. The derivative thermogravimetry (DTG) curve indicates that the oxidation of Cu NWs undergoes two processes, that is, the formation of Cu_2O and CuO around 240 and 310 ℃, respectively. When coated with Ni shell, the NWs become more stable in air and their oxidation starts from 270 ℃. The DTG curve shows that the boundary between Cu and Ni oxidation is not clearly defined together. With increasing Ni content, the onset oxidation of NWs shifts to high temperature, as indicated in Fig. 3b and Fig. S4†, further indicating the stability of Ni is higher than Cu. It is interesting to note that the weight gain increases from 21.5 % for Cu-Ni (3.5 : 1) NWs to 25.2 % for Cu-Ni (1: 3.3) NWs. Theoretically, the total oxidation of pure Cu and Ni should result in 25% and 27.3% weight increase, respectively. The negative deviation in experiments should result from the unavoidable oxide layer on these NWs as revealed by HRTEM images and EDS maps. The higher Ni content gives a smaller negative deviation, reflecting that Ni coating dramatically decreases the proportion of oxidized species.

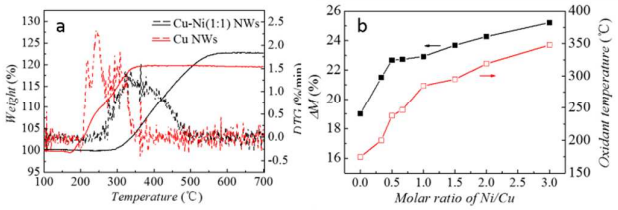

Fig3. (a) TG (dashed line) and DTG (solid line) curves of neat Cu NWs and Cu-Ni(1:1) NWs; (b) Plots of the onset oxidation temperature and weigh gain *versus* Cu/Ni molar ratio in nanowire.

To prepare flexible TCFs, Cu-Ni NWs were spray-coated onto a PET substrate heated at 120° C. Fig. 4a shows the photo of Cu-Ni(1:1) TCF, whose transmittance (*T*) is 76% and sheet resistance (*Rs*) is 300 Ω /sq. On PET substrate, the NWs are dispersed well without agglomeration, forming a percolation conductive network (Fig. 4b). The mechanical property of this TCF was examined by bending tests (Fig. S5†). Like high flexible Ag NW and Cu NW films, the Cu-Ni NW TCF almost keeps its resistance unchanged after 1000 time tension and compression bends. As known, the density of NWs, which could be changed by varying ink concentration, determines the conductivity of the network. For example, with increasing the density of Cu-Ni(1:1) NWs, the *T* and *Rs* of the corresponding TCFs decrease from 90 % to 60 % and 1M Ω /sq to 100 Ω /sq, respectively (Fig. 4c). For other Cu-Ni NWs, the *Rs* and *T* of their derived TCFs can also be tuned using similar procedure (Fig. S6†), and the results measured from each type of TCF are plotted in Fig. 4d. It is seen that the NWs with higher Ni content give rise to lower conductivity at the same *T*. In contrast to oxidation resistance, the conductivity of nickel (10^6 S m^{-1}) is half of that of copper (2×10^6 S m^{-1}), so thick Ni layer is not welcome. In addition, high content Ni will induce low aspect ratio and coarse surfaces of the one-pot synthesized Cu-Ni NWs, both of which can deteriorate the quality of final TCFs. On the other hand, to further increase the conductivity, Cu-Ni NWs are required to have small diameter, high aspect ratio, high crystallinity and less surface defects.[38, 39] Considering all the factors including stability, transparency and conductivity, we selected Cu-Ni(1:1) NWs as the optimal building blocks to make flexible heaters for defrosting windows.

Fig. 5 a and b depict time-dependent temperatures of two types of NW-based heaters prepared by using neat Cu NWs and Cu-Ni(1:1) NWs and operated at voltage of 3-15 V . The *Rs* of both heaters are controlled to be 300 Ω /sq and their sizes are 4 × 2 cm^2. The voltage to the film heaters is provided by a DC power supply through a copper contact at the film edge and the temperature response is monitored by an infrared camera. Within input voltage of 6 V, both Cu NW heater and Cu-Ni(1:1) NW heater display similar heating rate and reach steady state around 80 s. The temperature they reached under 6 V is around 41 °C. As the voltage is increased to 9 V, the Cu-

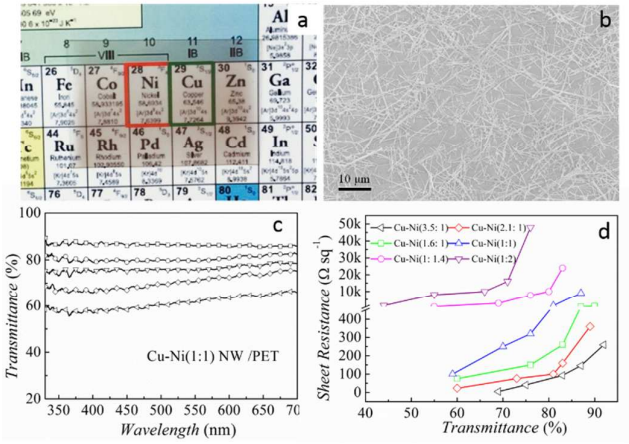

Fig4. (a) Photograph of Cu-Ni(1:1) TCF with *R* = 300 Ω sq^{-1} and *T* = 76 %; (b) SEM image; (c) Transmittance spectra of Cu-Ni(1:1) TCFs prepared by varying spay times, (d) Plots of sheet resistance *versus* transmittance for each type of TCF with tunable NW loading.

Ni NW heater elevates its steady-state temperature to 71.5 °C while the Cu NW device exhibits a quick heating at beginning stage (< 35 s) and then fails to rise its temperature any more. This failure on Cu NW device becomes more obvious when the working voltage is increased to 12 V under which the temperature is almost linearly risen to 63 °C and drops down afterwards. The breakdown point appears at Cu NW heaters because of the oxidation and even fusion of some Cu NWs. The breakdown point can be directly observed from its infrared image (Fig. S7†). The excellent stability owned by Cu-Ni(1:1) NWs allows the resulting flexible heaters to readily operate at 12 V and even up to 15 V. The saturated stable temperatures at 12 and 15 V are 87 and 106 °C, respectively. Moreover, most area over Cu-Ni(1:1) NW heater exhibits uniform color distribution (Fig. S7†), indicating the uniform heat distribution over the film. To further demonstrate the potential application of Cu-Ni(1:1) NW heater as a defrosting window, the NW film is sealed by a thin layer of polydimethylsiloxane (PDMS) with thickness of 50 μm to avoid short circuit current induced by water droplets (Fig. 5c). This PDMS protected heater is covered fully by frost after staying in a refrigerator for 30 min (Fig. 5d). After 12 V is applied to the heater for 2 min, the frost is completely removed, and the symbols below the heater become clearly visible (Fig. 5e). Therefore, Cu-Ni NWs enable us for the first time to construct flexible transparent heaters using non-precious metal NWs, which not only demonstrates the high quality of the optimal Cu-Ni NWs but also brings possibility to produce low-price transparent, flexible heaters.

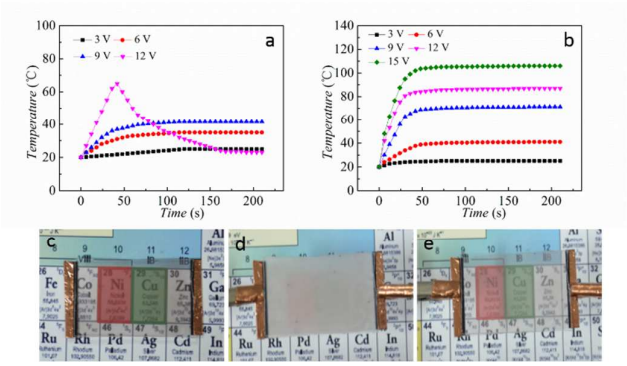

Fig5. Time dependent temperature profiles of (a) Cu NW heater and (b) Cu-Ni NW heater. Defrosting test of PDMS protected Cu-Ni NW heater: (c) pristine heater, (d) frosted, (e) defrosted.

Conclusions

We have developed one-pot synthesis of Ni-coated Cu NWs with tunable Ni-shell thickness by controlling their mole ratios in precursor. With increasing Ni content, the resulting Cu-Ni NWs increase their oxidation resistance while decrease the conductivity and transparency of their solution processed films. The optimal Cu-Ni NWs are prepared from Cu^{2+}/Ni^{2+} molar ratio of 1/1, allowing their derived TCFs to have T = 76 %, Rs = 300 Ω /sq and oxidation onset temperature up to 270 °C. Consequently, the NW heater made from Cu-Ni(1:1) NW TCF exhibits a quick temperature response and uniform heat distribution, and demonstrates effective defrosting capability, providing a potential to make flexible heaters and smart windows using low-price metal nanowires.

Acknowledgements

This work is jointly supported by Priority Academic Program Development of Jiangsu Higher Education Institutions (YX03001), Jiangsu National Synergetic Innovation Center for Advanced Materials (SICAM), Synergistic Innovation Center for Organic Electronics and Information Displays, Jiangsu Provincial NSF (BK20141424), Qing Lan Project of Jiangsu Province.

Notes and references

1. D. S. Hecht, L. Hu and G. Irvin, *Adv. Mater.* , 2011, **23**, 1482-1513.
2. K. Ellmer, *Nat. Photonics* 2012, **6**, 808-816.
3. D. S. Hecht and R. B. Kaner, *MRS Bull.* , 2011, **36**, 749-755.
4. S. Ye, A. R. Rathmell, Z. Chen, I. E. Stewart and B. J. Wiley, *Adv. Mater.* , 2014, **26**, 6670-6687.
5. S. De, P. J. King, P. E. Lyons, U. Khan and J. N. Coleman, *ACS Nano*, 2010, **4**, 7064-7072.
6. D. Angmo, T. R. Andersen, J. J. Bentzen, M. Helgesen, R. R. Søndergaard, M. Jørgensen, J. E. Carlé, E. Bundgaard and F. C. Krebs, *Adv. Funct. Mater.* , 2015, DOI: 10.1002/adfm.201501887
7. L. Hu, H. S. Kim, J.-Y. Lee, P. Peumans and Y. Cui, *ACS Nano*, 2010, **4**, 2955-2963.
8. S. J. Lee, Y.-H. Kim, J. K. Kim, H. Baik, J. H. Park, J. Lee, J. Nam, J. H. Park, T.-W. Lee, G.-R. Yi and J. H. Cho, *Nanoscale*, 2014, **6**, 11828-11834.
9. D.-S. Leem, A. Edwards, M. Faist, J. Nelson, D. D. C. Bradley and J. C. de Mello, *Adv. Mater.* , 2011, **23**, 4371-4375.
10. X.-Y. Zeng, Q.-K. Zhang, R.-M. Yu and C.-Z. Lu, *Adv. Mater.* , 2010, **22**, 4484-4488.
11. H. Lee, D. Lee, Y. Ahn, E.-W. Lee, L. S. Park and Y. Lee, *Nanoscale*, 2014, **6**, 8565-8570.
12. K.-H. Ok, J. Kim, S.-R. Park, Y. Kim, C.-J. Lee, S.-J. Hong, M.-G. Kwak, N. Kim, C. J. Han and J.-W. Kim, *Sci. Rep.*, 2015, **5**, 9464.
13. M.-G. Kang, T. Xu, H. J. Park, X. Luo and L. J. Guo, *Adv. Mater.* , 2010, **22**, 4378-4383.
14. M. Song, D. S. You, K. Lim, S. Park, S. Jung, C. S. Kim, D.-H. Kim, D.-G. Kim, J.-K. Kim, J. Park, Y.-C. Kang, J. Heo, S.-H. Jin, J. H. Park and J.-W. Kang, *Adv. Funct. Mater.* , 2013, **23**, 4177-4184.
15. J.-H. Lee, H.-S. Shin, Y.-J. Noh, S.-I. Na and H.-K. Kim, *Sol. Energy Mater. Sol. Cells*, 2013, **114**, 15-23.
16. A. R. Madaria, A. Kumar and C. Zhou, *Nanotechnology*, 2011, **22**. 245201.
17. J. Lee, P. Lee, H. Lee, D. Lee, S. S. Lee and S. H. Ko, *Nanoscale*, 2012, **4**, 6408-6414.
18. S. Kiruthika, R. Gupta and G. U. Kulkarni, *RSC Adv.*, 2014, **4**, 49745-49751.
19. C. Celle, and C. Mayousse, *Nano Res.*, 2012, **5**, 427-433.
20. S. Magdassi, M. Grouchko and A. Kamyshny, *Materials*, 2010, **3**, 4626-4638.
21. S. Ye, A. R. Rathmell, I. E. Stewart, and Y.-C. Ha, A. R. Wilson, Z. Chen and B. J. Wiley, *Chem. Commun.* , 2014, **50**, 2562-2564.
22. A. R. Rathmell and B. J. Wiley, *Adv. Mater.* , 2011, **23**, 4798-4803.
23. H. Guo, N. Lin, Y. Chen, Z. Wang, Q. Xie, T. Zheng, N. Gao, S. Li, J. Kang, D. Cai and D.-L. Peng, *Sci. Rep.*, 2013, **3**, 2323.
24. J. Song, J. Li, J. Xu and H. Zeng, *Nano Lett.* , 2014, **14**, 6298-6305.
25. Y. Chang, M. L. Lye and H. C. Zeng, *Langmuir*, 2005, **21**, 3746-3748.
26. A. R. Rathmell, N. Minh, M. Chi and B. J. Wiley, *Nano Lett.* , 2012, **12**, 3193-3199.
27. I. E. Stewart, A. R. Rathmell, L. Yan, S. Ye, P. F. Flowers, W. You and B. J. Wiley, *Nanoscale*, 2014, **6**, 5980-5988.
28. Z. Chen, S. Ye, I. E. Stewart and B. J. Wiley, *ACS Nano*, 2014, **8**, 9673-9679.
29. Z. Chen, A. R. Rathmell, S. Ye, A. R. Wilson and B. J. Wiley, *Angew. Chem. Int. Ed.*, 2013, **52**, 13708-13711.
30. Z. Chen, S. Ye, A. R. Wilson, Y.-C. Ha and B. J. Wiley, *Energy Environ. Sci.,* 2014, **7**, 1461-1467.
31. S. Zhang and H. C. Zeng, *Chem. Mater.* , 2010, **22**, 1282-1284.
32. J. Chen, W. Zhou, J. Chen, Y. Fan, Z. Zhang, Z. Huang, X. Feng, B. Mi, Y. Ma and W. Huang, *Nano Res.*, 2015, **8**, 1017-1025.
33. Z. Xu, E. Lai, Y. Shao-Horn and K. Hamad-Schifferli, *Chem. Commun.*, 2012, **48**, 5626-5628.
34. J. Feng and C. P. Zhang, *J. Colloid Interface Sci.,* 2006, **293**, 414-420.
35. S. Zhang and H. C. Zeng, *Chem. Mater.* , 2009, **21**, 871-883.
36. H. Guo, Y. Chen, H. Ping, J. Jin and D.-L. Peng, *Nanoscale*, 2013, **5**, 2394-2402.
37. D. Zhang, R. Wang, M. Wen, D. Weng, X. Cui, J. Sun, H. Li and Y. Lu, *J. Am. Chem. Soc.* , 2012, **134**, 14283-14286.
38. J. S. Jang, U. A. Joshi and J. S. Lee, *J. Phys. Chem. C.*, 2007, **111**, 13280-13287.
39. J. Tang, Z. Huo, S. Brittman, H. Gao and P. Yang, *Nat. Nanotech.*, 2011, **6**, 568-572.

Journal Name

ARTICLE

Table of Contents